J Mater Sci (2009) 44:5332–5338
DOI 10.1007/s10853-009-3538-0

FERROELECTRICS

# A post-growth processing methodology to achieve barium strontium titanate thin films with low dielectric loss and high tunability for reconfigurable tunable devices

**Melanie W. Cole · Adrian Podpirka · Shriram Ramanathan**

Received: 5 April 2009 / Accepted: 2 May 2009 / Published online: 21 May 2009


**Abstract** $Ba_{0.60}Sr_{0.40}TiO_3$ (BST) thin films, grown via RF-sputtering and the metalorganic solution deposition (MOSD) techniques, were post-growth annealed via conventional thermal annealing (CTA) and UV-photon irradiation annealing. With respect to the conventional thermal annealed films the UV-photon irradiation annealed films possessed improved structural properties and dielectric response. The optimization of the UV-photon irradiation annealing process parameters (using RF-sputtered BST films) was achieved via a detailed set of iso-thermal/chronal annealing experiments. The optimized UV-process parameters, applied to MOSD synthesized BST films revealed further enhanced dielectric response, i.e., 23% reduction in tan $\delta$ with sustained tunability of 42%. The improvements in the material properties of the UV-photon irradiation annealed BST thin films are attributed to stoichiometry and structural changes enabled through the UV-photon irradiation annealing process.

## Introduction

Frequency-agile or reconfigurable components are becoming increasingly important and/or necessary to cope with a multitude of signal frequencies and modulation formats in a variety of communication systems. A critical challenge is to develop a Ka-band ($\sim$26–40 GHz) tunable RF filter technology that holds promise to reduce bit-error rates in satellite communications, improve performance of close-range targeting radars, and allow for more information to be sent through limited-bandwidth channels.

Most tunable filters described in the literature fall into three basic types: mechanically tunable, magnetically tunable, and electronically tunable filters [1]. The major issue with current tunable filter technologies is that their performance above 10 GHz falls short of end user performance requirements. Due to their low tuning speed and poor reliability mechanically tunable filters are not viable for advanced communications systems. Both semiconductor and magnetic based materials have been extensively researched for electronic and magnetically tunable filters, respectively. Magnetically tunable filters using yttrium–iron–garnet (YIG) are very popular because of their multi octave tuning range, very high sensitivity, spurious-free response, and compact size [1, 2]. However, due to the low saturation magnetization (Ms) of YIG ($4\pi Ms = 1.75$ kG) the operating frequency of YIG filters has been limited to low frequencies (<10 GHz). However, recent work focused on high Ms materials such as Fe ($4\pi Ms = 21.5$) and permalloy ($4\pi Ms = 10$ kG) has received attention for tunable filter applications although promising, these technologies are still in early stages and further study is needed to achieve the required Ka-band tunable filter performance criteria [1, 3]. Most of the electronically tunable filters use semiconductor, GaAs, and varactor diodes. The varactor diode capacitance varies with reverse voltage; when a varactor is in series with a resonator circuit or element, this capacitance change alters the resonant frequency. Semiconductor varactor diodes and PIN (*p*-type, intrinsic, and *n*-type) diodes have a relatively large quality factor "*Q*"

M. W. Cole (✉)
U.S. Army Research Laboratory, Weapons and Materials Research Directorate, Aberdeen Proving Ground, Aberdeen, MD 21005, USA
e-mail: mcole@arl.army.mil

A. Podpirka · S. Ramanathan
School of Engineering and Applied Sciences, Harvard University, Cambridge, MA 02138, USA

(a measure of the ratio of power stored in a device to the power lost by it) below 10 GHz, however, the $Q$ drops down drastically above 10 GHz making them less attractive for applications above 10 GHz. In addition to high losses above 10 GHz, GaAs varactor diodes also a have low power handling capability.

The recent drive toward developing "affordable" electronically tunable RF components has stimulated enormous interest in designing tunable RF devices utilizing perovskite oxides, $Ba_xSr_{1-x}TiO_3$ (BST) based thin films [4]. BST based varactors possess many excellent attributes which include fast switching speed (intrinsically fast $\approx$ ns), good power handling capabilities (>1 W), low DC power consumption ($\ll$1 μA current) μW, very small size (parallel plate varactor $\sim mm_2$) and high dielectric tunability (>2:1). These performance metrics are very desirable for tunable filter technology; hence promoting BST thin films as promising candidates for tunable filters. The possibility of using BST thin film varactors in tunable filters has been recognized for quite sometime, unfortunately this application space has not been fully exploited since most filter applications place a high premium on insertion-loss in the pass-band while maintaining high tunability. To date, the technology for BST fabrication has not been able to satisfy the required balance of these two material properties while still maintaining excellent reliability and device affordability. Conventional approaches for lowering thin film BST dielectric loss include: alio-valent doping [5–8], film stress modification [9, 10], texturing [11], ferroelectric-low loss oxide material layering [12], and improving the film/electrode interface quality by adding buffer layers between the film and bottom electrode [13]. Although successful at lowering dielectric loss, these approaches unfortunately often lead to severe degradation of the films' tunability and frequently involve complex non industry-standard film processing steps. There is a critical need to develop new material designs and/or film processing methods that enable maintenance of BST $Q$-factor (low dielectric loss/insertion loss) without compromising the material tunability ($\eta = 2{:}1$) and other required filter performance metrics, such as device impedance matching ($\varepsilon_r < 500$), film resistivity/conductivity (leakage current $\sim$ milliampere range) and long-term reliability (long-term performance under extended applied voltage and temperature).

In this article, we report on the development of a post-growth ultraviolet (UV)-photon irradiation annealing process science protocol which serves to improve the quality factor ($Q$) and leakage characteristics ($I_L$) of complex multi-component dielectric films while sustaining high dielectric tunability. We have synthesized $Ba_{1-x}Sr_xTiO_3$, (BST) thin films using a combinational processing technique, which blended radio frequency (RF)-sputtering and/or metalorganic solution deposition (MOSD) film fabrication and photon irradiation annealing to achieve balanced BST material properties, i.e., property enhancement without degradation of required performance metrics. UV photon illumination is an elegant approach to modulate properties of thin film oxides, particularly enabling controlled incorporation of oxygen into the oxide in a self-limiting manner [14]. In this study, we discuss briefly our results on this non-complex, affordable processing route for fabricating tunable, active thin film oxides that satisfies the requirements for the balanced competing material properties of low dielectric loss and high tunability.

## Experimental procedure

The experiments consisted of two parts, Experimental Set I and II. The first set of films, Experimental Set I, were synthesized via RF-sputtering and were utilized to determine the baseline parameters for the UV-photon irradiation annealing methodology. The second set of experiments, Experimental Set II, applied the optimized UV-photon irradiation annealing baseline parameters (obtained in Experimental Set I) to BST films which were optimized for stoichiometry, microstructure, surface morphology, and dielectric response via the MOSD synthesis route [7]. The film processing methodologies for both sets of experiments are described below.

### Experimental data set I

The $Ba_{0.60}Sr_{0.40}TiO_3$ (BST (60/40)) thin films ($\sim$100 nm thickness) were RF sputtered from a stoichiometric $Ba_{0.60}Sr_{0.40}TiO_3$ ceramic target onto platinized silicon wafers and $r$-plane sapphire substrates. The as-deposited films were annealed via conventional thermal annealing (CTA) and UV-photon irradiation annealing. Both sets of films were in situ annealed at variable temperatures (600–800 °C) and times (15–225 min) in a custom built load lock annealing chamber connected to the sputtering chamber. The annealing chamber was designed with a substrate heater and precision oxygen partial pressure control, and equipped with an in situ photon sources facing the sample for performing UV-assisted annealing. The UV photon source is an Hg-vapor lamp array which produces radiation between 185 and 254 nm.

### Experimental data set II

BST (60/40) thin films of the same composition as those in Experimental Set I were synthesized by MOSD, the experimental details of film synthesis are presented elsewhere [7]. The as-grown films were annealed via conventional thermal annealing (CTA) and UV-photon irradiation

annealing the using the optimized UV-photon irradiation annealing parameters achieved in Experimental set I. Specifically, the optimized baseline UV annealing parameters used were determined to be 700 °C with annealing times between 50 and 75 min.

The structure of the BST films was characterized via Glancing Angle X-Ray Diffraction (GAXRD) via a Scintag XDS 2000 diffractometer. The film capacitance $C_p$ and dissipation factor (tan $\delta$) were measured in the metal–insulator–metal (MIM) device configuration using Pt top and bottom electrodes via an Agilent 4284a LCR meter. The dielectric constant was calculated from the capacitance measured at a frequency of 100 kHz. The insulating properties of the films were evaluated via current–voltage measurements using a semiconductor probe station. Cross-sectional film microstructure was examined using a Hitachi S4500 field emission scanning electron microscope (FESEM) and the surface morphology of the films was assessed by a Digital Instrument's Dimension 3000 atomic force microscope (AFM) using tapping mode.

## Results and discussion

The as-deposited RF-sputter deposited BST films, grown on *r*-plane sapphire and Pt/Si substrates were annealed for 60 min at temperatures ranging from 615 to 783 °C with and without UV treatment in an oxygen environment. As-deposited films were found to be amorphous from X-ray diffraction. The annealed films showed no evidence of secondary phase formation, as no peaks other than (100), (110), (111), (200), and (211) BST peaks were observed from X-ray diffraction as seen in Fig. 1 with the bulk values given by the vertical lines [15]. For the CTA films, there was a slight shift of the X-ray peaks to lower angles (corresponding to larger interplanar spacing) with respect to that of the UV-photon irradiation annealed BST films. This shift in the peak position is indicative of the fact that the lattice parameter of the conventionally thermal annealed BST films, based on the (110) X-ray peak, i.e., at 700 °C $a_{\text{conventional anneal}} = 4.01$ Å as opposed to $a_{\text{UV-assisted anneal}} = 3.99$ Å, was larger than that for the UV-photon irradiation annealed films. Figure 2 shows the calculated lattice parameter from the (110) peak as a function of temperature for the two set of samples. The dotted-dashed line in Fig. 2 represents the lattice parameter for bulk ceramic $Ba_{0.60}Sr_{0.40}TiO_3$, (3.9650 Å) [15]. The UV-treated films display characteristics closer to that of bulk BST, i.e., lattice parameter closer to bulk with respect to the conventional thermal annealed BST film. Oxygen vacancies affect nearest neighbor distance by reducing the Coulomb attractive force in the ionic lattice, resulting in an increased lattice parameter [16]. The presence of activated

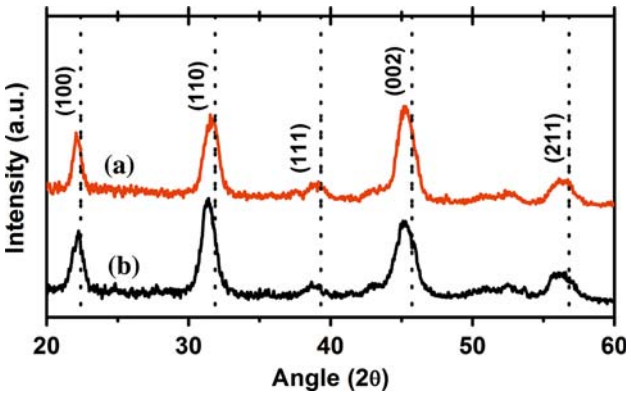


**Fig. 1** Glancing incidence XRD patterns of BST thin films annealed at 700 °C for 60 min: (*a*) with UV treatment; and (*b*) without UV treatment. *Dotted lines* represent the BST (60/40) bulk peak position [15]

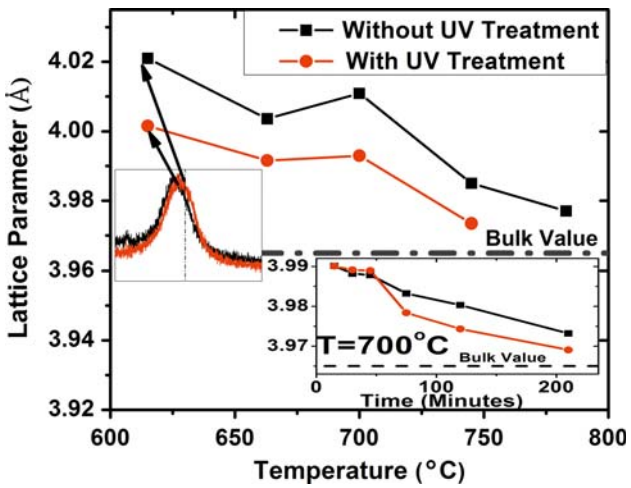


**Fig. 2** Change in lattice parameter as a function of annealing temperature for BST films annealed with (*filled circles*) and without (*filled squares*) UV-assist. Inset shows the Change in lattice parameter as a function of annealing time at 700 °C for BST films annealed with (*filled circles*) and without (*filled squares*) UV-assist. *Dotted lines* represent the BST (60/40) bulk lattice parameter [15]

oxygen in the near-surface vicinity during UV annealing allows for a greater compensation of the vacancies thereby likely resulting in the reduction of the lattice parameter [17].

Both sets of films were annealed at 700 °C as a function of annealing time ranging from 15 to 225 min. The inset in Fig. 2 displays the variation in lattice parameter as a function of annealing time for films annealed at 700 °C with and without UV assist. After annealing for ~45 min there is a divergence in the lattice parameter such that at the same annealing time the lattice parameter of the UV assist annealed film has contracted substantially with respect to that of the non-UV annealed film and hence the

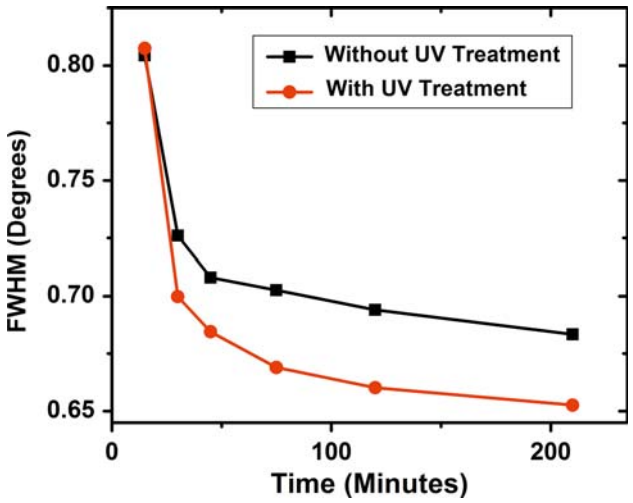


**Fig. 3** Variation in full width at half maximum (FWHM) of the (110) peak annealed at 700 °C of UV assisted (*filled circles*) and non-UV treated (*filled squares*) BST (60/40) films as a function of annealing time

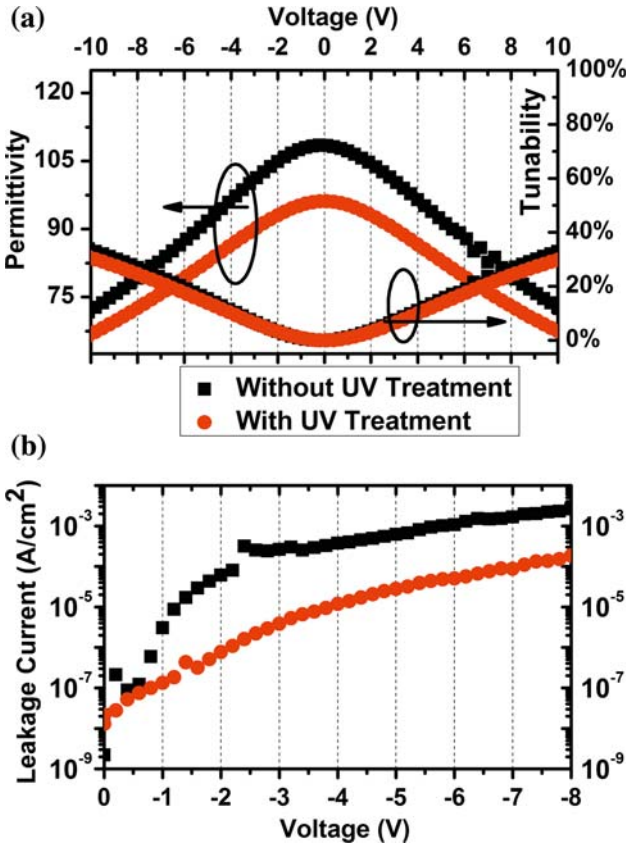


**Fig. 4** **a** Dielectric response as a function of applied bias for the BST films annealed at 700 °C with (*filled circles*) and without UV-assist (*filled squares*). **b** Variations of leakage current density with applied bias for the BST thin films annealed at 700 °C with (*filled circles*) and without UV-assist (*filled squares*)

lattice parameter is closer to that of bulk BST. This result suggests that UV irradiation has a dramatic effect on the film structure whereby, the more pronounced lattice parameter contraction observed for the UV treated films advocates that UV irradiation leads to a reduction in oxygen vacancies, hence yielding lower residual stress in the UV-annealed film. Figure 3 shows the change in full width at half maximum (FWHM) of the BST films annealed with and without UV-photon irradiation, respectively. The steep decrease in FWHM, observed for both sets of films, as the time is increased from 15 to 30 min, suggests an increase in the grain size over a relatively short time interval. The fact that the UV-treated film showed a larger decrease in FWHM with respect to the non-UV-treated film suggests that the UV-irradiation enhances film crystallinity.

Figure 4a displays the permittivity and tunability of the two sets of films as a function of applied bias. The maximum permittivity of the UV annealed ($\varepsilon v = 0 = 96$) BST film is in a similar range as that of the non-UV annealed film annealed ($\varepsilon v = 0 = 108$). The permittivity for both sets of films is reasonable (i.e., $\varepsilon r < 500$), for device impedance matching purposes [18]. The tunability data is important, whereby tunability ($\eta$) is defined as $\eta = \Delta C/C_0$ and $\Delta C$ is the change in capacitance relative to zero-bias capacitance $C_0$ [6]. Figure 4a shows that the tunability exhibits non-hysteretic behavior, indicating the paraelectric phase and is virtually the same for both annealing treatments, with a maximum of $\sim$36% at $\pm$10 V applied bias. However, the tunability value is somewhat lower than desired for practical tunable device/filter applications. Literature values of tunability for RF sputtered BST films have been reported to be as high as 70% [19]; thus our moderate value of film tunability, $\sim$36% at $\pm$10 V applied bias, may be attributed to the fact that the initial deposition parameters for the RF-sputtered film synthesis are not fully optimized. The measured dielectric loss for both sets of films established that the dissipation factor was also somewhat high $\sim$5% (attributed to non-optimized sputter deposition process parameters), however, the dielectric loss the UV-treated film was found to be reduced by $\sim$20% with respect to that of the non-UV treated film. Regardless of the absolute value of tunability and dielectric loss, what is critical is the trend observed in this data set. In other words, the UV-photon irradiation annealing served to reduce the dielectric loss while maintaining a tunability which was equivalent to that of conventional thermal processed BST films, hence achieving loss reduction without degrading the dielectric tunability. The dielectric response data appears consistent with the lattice parameter findings and is in support of the UV-assist's consequence to mitigate oxygen vacancies, thereby resulting in improved dielectric loss [20].

Leakage current characteristics of BST thin films were measured using MIM capacitors. The leakage current density as a function of applied bias is shown for both the

UV assist and thermally annealed BST films in Fig. 4b. In contrast to conventional thermal annealing, the UV-photon irradiation annealed BST film has a significantly lower leakage current density under reverse bias (with reference to top electrode). As an example of the reduction of leakage current, the current density of the UV-assist annealed BST film is $7.73 \times 10^{-7}$ Å/cm$^2$ at $-2.0$ V applied bias and this value is significantly lower than that for the conventional thermal annealed film ($6.11 \times 10^{-5}$ Å/cm$^2$) for the same electric field. The oxygen vacancies within the film act as electron trap sites causing high leakage currents in the Pt/BST/PT capacitor structure [21]. The UV-photon irradiation annealing process increases oxygen incorporation into the oxide film passivating oxygen vacancies and resulting in a reduction of the leakage currents. Tsuchiya et al. [22] have recently shown that photon irradiation even as low as room temperature can enable oxygen concentration enhancements of the order of few percent in thin film oxides and the fact that leakage currents decrease upon photon illumination suggest that the compensation mechanisms are primarily due to filling oxygen vacancies.

The isothermal, isochronal, and post-growth UV-photon irradiation annealing experimental data described above served to define the base-line parameters and processing limits for achieving an optimized UV-photon irradiation annealing process protocol. The data suggest that there are kinetic considerations for achieving UV-photon irradiation annealing process parameter optimization. Based on the film's structural response (maximum contraction of the lattice parameter and minimization of the X-ray peak FWHM) the optimum UV-post growth processing thermal window was determined to be between 650 and 750 °C and the time or process duration, should be greater than 45 min. It must, however, be kept in mind that both the thermal and temporal UV-processing windows may require modification to account for differences in film thickness and/or microstructure, and as such, the process windows determined in this study should be treated as a baseline optimization for the UV-photon irradiation annealing process.

The base-line parameters for the UV-photon irradiation annealing process were applied to BST films synthesized via MOSD. The MOSD BST films were annealed via CTA (700 °C for 60 min in oxygen ambiance) and via UV-assist annealing at 700 °C for 60 min. As in the case of the RF sputtered BST films, the XRD structural studies revealed a down shift (larger interplanar spacing) in the X-ray peaks of the MOSD fabricated BST film which were CFA versus that of the UV treated films. This downshift in the peak position is indicative of the fact that the lattice parameter of the conventional thermal annealed BST films, based on the (110) X-ray peak, i.e., at 700 °C $a_{\text{conventional anneal}} = 4.00$ Å as opposed to $a_{\text{UV-assisted anneal}} = 3.97$ Å, was slightly larger than that for the film annealed with the UV-photon irradiation process. The fact that the lattice parameter of the UV treated film is closer to that of bulk BST60/40 (3.9650 Å) suggests that UV treated film possess less stress.

The film microstructure, in the direction normal to the film surface, was analyzed via cross-sectional FESEM. The cross-sectional FESEM micrographs of the UV treated films, displayed in Fig. 5, showed that the BST films possessed a dense well-crystallized microstructure with a uniform cross-sectional thickness of 100 nm. The films were polycrystalline and were composed of grains randomly distributed throughout the film thickness. This film microstructure is typical of chemically fabricated films [7, 23]. The FESEM micrograph shows a distinct structural delineation between the film and the bottom electrode stack (Pt/Ti). No amorphous layer or voiding/defects was observed at the film–electrode interface. This defect free and structurally abrupt interface bodes well for the films excellent interfacial integrity, which in turn should be reflected in the dielectric response.

The surface morphology of the CTA and UV treated BST films was assessed via tapping mode AFM over a $1 \times 1$ μm$^2$ scan area (Fig. 5b, c). The AFM results determined the RMS surface roughness to be 3.0 nm and 2.66 nm for the UV treated and CFA films, respectively. The parameter of film surface roughness is important for device performance since the dielectric properties depend not only on a well-defined microstructure, but also on the quality of the electrode (required for microwave devices)–

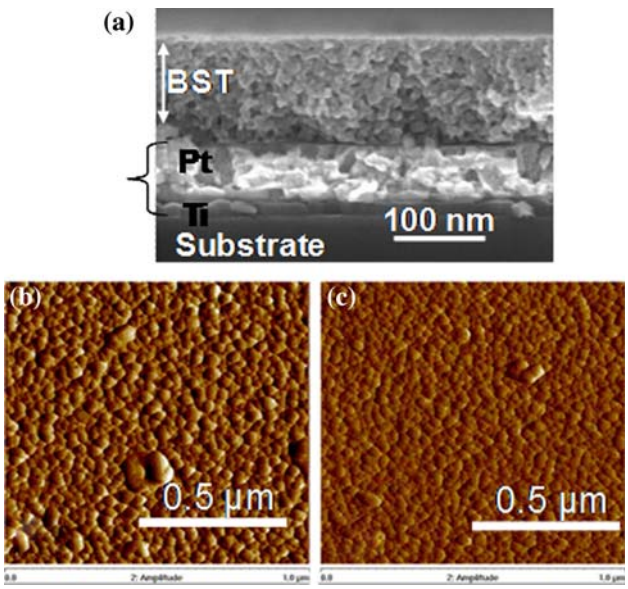


**Fig. 5** MOSD grown BST films: **a** FESEM cross-section micrograph of the 700 °C/60 min. UV-photon irradiation annealed film. AFM images of the MOSD grown BST film crystallized via **b** UV-irradiation annealing and **c** conventional thermal annealing at 700 °C for 60 min

film interface [24]. Values of surface roughness less than 4 nm are acceptable for tunable device applications. Figure 5b shows that both sets of films exhibited a dense microstructure with no cracks or defects observed. However, the UV treated film (Fig. 5b) is larger grained, hence possesses a more fully developed crystalline microstructure with respect to that of the CTA–BST film (Fig. 5c). The fact that the UV-treated BST film is more fully developed than the CTA film at the same annealing temperature/time suggests that UV treatment would be useful in reducing the overall BST processing temperature. Reduced processing temperatures, balanced with the maintenance of good stoichiometry and crystallinity, may be beneficial for CMOS integration. In addition, lower process temperatures also have a significant influence on reducing the strain in the film.

Figure 6 displays the dielectric response as a function of measured frequency for both sets of BST films. The dielectric properties did not show any appreciable dispersion with measured frequency up to 1 MHz indicating good film quality and the absence of internal interfacial heterogeneities. The measured small signal dielectric constant at 100 kHz for both films were similar, i.e., $\varepsilon_r = 260$ (UV-treated BST) and $\varepsilon_r = 256$ (CTA BST). In contrast to the permittivity data, there was a notable difference in the loss factor, whereby the dielectric loss was appreciably lower ($\sim$23% lower) for the UV-treated film (tan $\delta = 0.017$,) with respect to that of the CTA film (tan $\delta = 0.022$). Figure 7 displays the dielectric tunability for the BST films. The tunability is virtually the same for both annealing treatments, showing maximum tunability of $\sim$42% at $E = 750$ kV/cm applied bias. The loss and tunability data trends for the MOSD films parallel those of the RF-sputtered films with the exception that the absolute

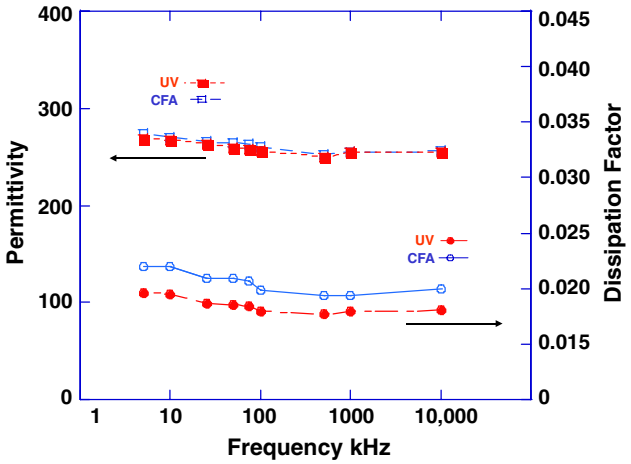


**Fig. 6** Dielectric response as a function of frequency for the BST films annealed at 700 °C/60 min with (*filled symbols*) and without UV-assist (*open symbols*)

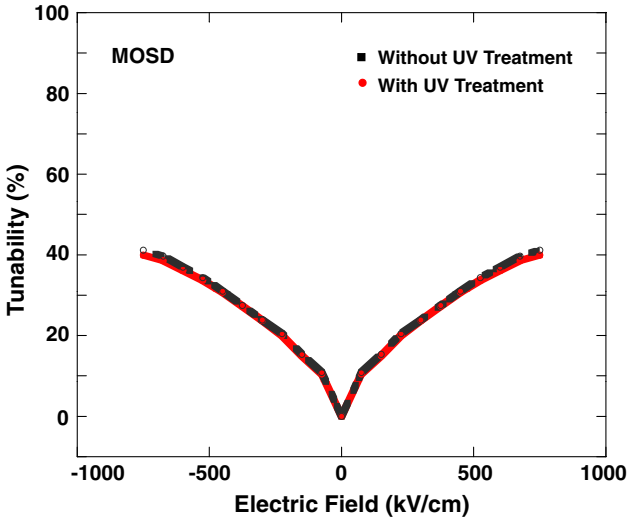


**Fig. 7** Tunability of the MOSD grown BST films annealed at 700 °C with (*filled circles*) and without UV-assist (*filled squares*)

value of dielectric loss was significantly lower and the tunability was higher than that for the RF-sputtered films. It is suggested that the improved dielectric response for the MOSD films with respect to that of the sputtered films is due to the fact that the initial film growth process parameters (pre-crystallization) of the MOSD fabricated films were better optimized than that of the RF-sputtered films, hence resulting in improved post-growth/annealed material properties.

The experimental data for the MOSD BST films clearly shows that UV-photon irradiation annealing served to reduce the loss tangent without degrading the film tunability, hence achieved material property balance (reduction of dielectric loss without degradation of tunability). The improved dielectric loss without degradation of tunability of the UV-treated MOSD grown BST films is important as the loss tangent serves to dissipate or absorb the incident microwave energy; thus the low loss tangent serves to decrease the insertion loss [25]. The retained high tunability allows for fewer tuning elements which are cascaded to achieve the desired tuning [26]. The decrease of the amount of tuning elements directly reduces the net circuit loss. Hence a low loss combined with a high tunability of the UV-treated MOSD fabricated BST thin films serves to enhance system performance.

## Conclusions

In conclusion, this study demonstrates the potential for utilizing photon irradiation assisted annealing to achieve desirable performance for electric-field tunable perovksite oxides such as (Ba,Sr)$TiO_3$. Specifically, the UV-assist annealed films possessed improved leakage current

characteristics and dielectric loss (hence, lowering the insertion loss of the device) with sustained tunabilities. The experimental data demonstrates that for equivalent time and temperature annealing conditions the UV-photon irradiation annealed films possessed a higher degree of crystallinity compared to conventionally annealed films suggesting that UV-assisted annealing may enable reduction in synthesis temperature/time and facilitate compatibility of BST thin film with CMOS technology.

## References


1. Uher J, Hoefer WJR (1991) IEEE Trans Microwave Theory Tech 39(4):643
2. Helszajn J (1985) YIG resonators and filters. New York, Wiley
3. Kuanr B, Harward IR, Marvin DL, Fal T, Camley RE, Mills DL, Celinski Z (2005) IEEE Trans Magn 41(10):3538
4. Vorobiev A, Rundqvist P, Khamchane K, Gevorgian S (2003) Appl Phys Lett 83(15):3144
5. Cole MW, Geyer RG (2004) Revista Mexicana De Fisica 50(3): 232
6. Cole MW, Geyer RG (2004) Mech Mater 36(10):1017
7. Cole MW, Hubbard C, Ngo E, Ervin M, Wood M, Geyer RG (2002) J Appl Phys 92:475
8. Cole MW, Joshi PC, Ervin MH, Wood MC, Pfeffer RL (2000) Thin Solid Films 374(1):34
9. Ban Z-G, Alpay SP (2003) J Appl Phys 93:504
10. Hyun S, Lee JH, Kim SS, Char K, Park SJ, Sok S, Lee EH (2000) Appl Phys Lett 77:3084
11. Kim HS, Hyun TS, Kim HG, Kim ID, Yun TS, Lee JC (2006) Appl Phys Lett 89:052902
12. Sahoo SK, Agrawal DC, Mohapatra YN, Majumder SB, Katiyar RS (2004) Appl Phys Lett 85:5001
13. Choi W, Kang BS, Jia QX, Matias V, Findikoglu AT (2006) Appl Phys Lett 88:062907
14. Ramanathan S, Chi D, McIntyre PC, Wetteland CJ, Tesmer JR (2003) J Electrochem Soc 150:F110
15. JCPDS Report No. 00-034-0411
16. Kim WJ, Chang W, Qadri SB, Pond JM, Kirchoefer SW, Chrisey DB, Horwitz JS (2000) Appl Phys Lett 76:1185
17. Podpirka A, Cole MW, Ramanathan S (2008) Appl Phys Lett 92:212906
18. Cole MW, Joshi PC, Ervin MH (2001) J Appl Phys 89(11):6336
19. Pervez NK, Hansen PJ, York RA (2004) Appl Phys Lett 85:4451
20. Horwitz JS, Chang W, Kim W, Qadri SB, Pond JM, Kirchoefer SW, Chrisey DB (2000) J Electroceram 4(2–3):357
21. Joo J-H, Seon J-M, Jeon Y-C, Oh K-Y, Roh J-S, Kim J-J (1997) Appl Phys Lett 70:3053
22. Tsuchiya M, Shutthanandan V, Engelhard MH, Ramanathan S (2008) Appl Phys Lett 93:263109
23. Wu Y, Jacobs EG, Pinizzotto RF, Tu R, Liu HY, Summerfelt SR, Grande BE (1995) Mater Res Soc Symp Proc 361:269
24. Pontes FM, Longo E, Leite ER, Varela JA (2001) Thin Solid Films 386(1):91
25. Wu L, Wu S, Chang F-C, Shen Y-T, Chen Y-C (2000) J Mater Sci 35:5945. doi:10.1023/A:1026722206381
26. Cole MW, Ngo E, Hirsch S, Demaree JD, Zhong S, Alpay SP (2007) J Appl Phys 102:034104